Title: Multiscale model of heart growth during pregnancy: Integrating mechanical and hormonal signaling

Authors:
Kyoko Yoshida[a*]
ky2p@virginia.edu; kyoko.yoshida@gmail.com

Jeffrey J. Saucerman[a,b]
jsaucerman@virginia.edu

Jeffrey W. Holmes[a,c]
holmesjw@uab.edu

Affiliations:
a: Department of Biomedical Engineering, University of Virginia, Charlottesville, VA 22908
b: Robert M. Berne Cardiovascular Research Center, University of Virginia, Charlottesville, VA 22908
c: School of Engineering, University of Alabama at Birmingham, Birmingham, AL 35294
*: Corresponding Author

Abstract

Pregnancy stands at the interface of mechanics and biology. The growing fetus continuously loads the maternal organs as circulating hormone levels surge, leading to significant changes in mechanical and hormonal cues during pregnancy. In response to these cues, maternal soft tissues undergo remarkable growth and remodeling to support both mother and baby for a healthy pregnancy. We focus here on the maternal left ventricle, which increases its cardiac output and mass during pregnancy. The objective of this study is to build a multiscale cardiac growth model for pregnancy to understand how mechanical and hormonal cues interact to drive this growth process. Towards this objective, we coupled a cell signaling network model that predicts cell-level hypertrophy in response to hormones and stretch, to a compartmental model of the rat heart and circulation that predicts organ-level growth in response to hemodynamic changes. Since pregnancy is associated with a volume overloaded state and elevated hormones, we first calibrated the coupled, multiscale model to data from experimental volume overload (VO) and hormonal infusion of angiotensin 2 (AngII), estrogen (E2), and progesterone (P4). We then validated the ability of our model to capture interactions between inputs by comparing model predictions against published observations for the combinations of VO+E2 and AngII+E2. Finally, we simulated pregnancy-induced changes in hormones and hemodynamics to predict heart growth during pregnancy. Our multiscale model produced realistic heart growth consistent with experimental data. Overall, our analysis suggests that much of heart growth during pregnancy is driven by the early rise in P4, particularly during the first half of gestation. We conclude with suggestions for future experimental studies that will provide a better understanding of how hormonal and mechanical cues interact to drive pregnancy-induced heart growth.

Keywords: Cardiac Hypertrophy, Estrogen, Progesterone, Volume Overload, Computational model, Systems biology
Funding: This work was supported by the National Institutes of Health (U01 HL127654).

1. Introduction

Pregnancy stands at the interface of mechanics and biology. Throughout nine months of pregnancy, the growing fetus continuously loads the maternal organs while circulating hormone levels surge. Pregnancy presents a cardiovascular challenge to the mother as her cardiac output increases by 45%, her total systemic resistance falls by 34%, and her total blood volume increases by almost 50% during a normal, singleton pregnancy [1,2]. Simultaneously, circulating estrogen (E2) and progesterone (P4) hormone concentrations increase up to 10 times above nonpregnant levels [3]. In response to these dynamic mechanical and hormonal cues, maternal soft tissues undergo significant growth and remodeling to support both mother and baby. We focus here on the maternal left ventricle (LV), which increases in mass and cavity volume by approximately 30% during the course of a normal pregnancy and regresses to normal size between 3-6 months after delivery [4].

Cardiovascular conditions and cardiomyopathy together account for more than 25% of pregnancy-related deaths [5]. With maternal death rates in the United States rising over the last 25 years [6], there is a critical need to understand how pregnancy hormones and hemodynamic changes interact to affect heart growth. Cardiac hypertrophy is a complex, multiscale process, driven by both mechanical and hormonal stimuli that interact through an extensive network of intracellular pathways within a cardiac muscle cell (cardiomyocyte). Experimentally, hypertrophy can be triggered by either hemodynamic or pharmacologic interventions. An increase in aortic resistance due to constriction (pressure overload, PO) leads to mass increase and wall thickening, while an increase in cardiac output due to an arteriovenous fistula or valvular regurgitation (volume overload, VO) leads to mass increase and LV cavity dilation. Infusion of isoproterenol leads to LV mass increase [7–18], as does infusion with angiotensin [19–26]. Pregnancy hormones also influence heart growth. Experimental studies have shown the ability of E2 to attenuate growth [27], and the role of P4 in promoting growth [28]. Furthermore, mechanical and hormonal stimuli can interact to impact growth, as demonstrated by attenuated LV mass increase in experiments of volume and pressure overload in E2 treated animals compared to untreated animals [29–35].

Computational models have made considerable progress in predicting heart growth in response to both hormonal and mechanical stimuli [36]. Computational systems biology models can predict cell-level cardiomyocyte growth in response to hormones and pharmaceutical interventions [37,38]. Mechanics-based growth models can predict heart growth at the organ level in multiple settings where changes in mechanical loading of the heart occur, including PO, VO, myocardial infarction, and dyssynchrony [39,40]. The objective of this work is to build a multiscale cardiac growth model for pregnancy by combining a systems biology model with a mechanics-based model to capture the interactions between hormonal and mechanical stimuli. Towards this objective, we created a cell signaling network model that predicts cell-level growth in response to the pregnancy hormones E2, P4, as well as angiotensin 2 (AngII), and stretch. We coupled this network model to a compartmental model of the rat heart and circulation to capture changes in hemodynamics. Because pregnancy is associated with both VO and elevated hormones, we first calibrated this multiscale model to match experimental heart growth in response to VO and infusions of AngII, E2, and P4. We then validated model predictions against experimental observations of heart growth in response to the combinations of AngII+E2 and VO+E2. Finally, we simulated pregnancy changes in hormones and hemodynamics to predict heart growth during pregnancy. Our multiscale model was able to capture reported pregnancy changes in both LV growth and hemodynamics. Furthermore, our analysis suggests that much of heart growth during pregnancy is driven by the early rise in P4, particularly during the first half of gestation. Together,

our model highlights the importance of both hormonal and mechanical effects on cardiac growth and function during pregnancy.

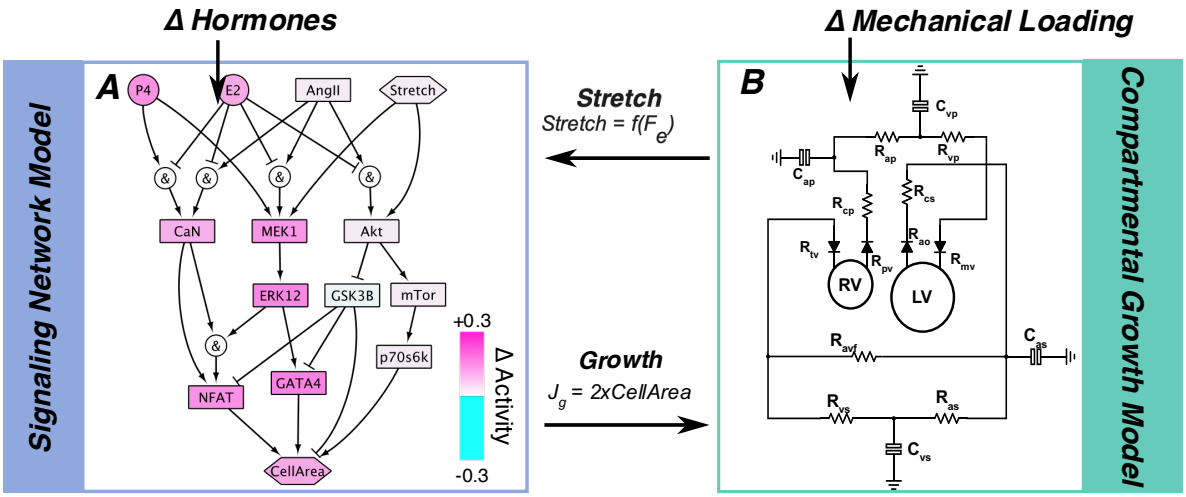

Figure 1: Multiscale cardiac growth model for pregnancy. A.) Intracellular signaling network model of cardiomyocyte growth is coupled to a B.) compartmental growth model. The network model predicts the amount of growth due to a particular level of hormones (P4, E2, AngII) and Stretch, and outputs a CellArea, which is fed into the compartmental model as a growth stretch. Colors represent an example of activity levels during pregnancy where pink represents increased activity and blue represents decreased activity compared to baseline. Changes in elastic stretches (F_e) due to growth and hemodynamic alterations are calculated in the compartmental model and fed back into the network model to close the loop.

2. Methods

2.1 Intracellular signaling network model of cardiomyocyte growth

To simulate the influences of hormones and stretch on cell-level growth, we built an intracellular signaling network model for cardiomyocyte hypertrophy (Fig. 1A). Our approach was similar to a model developed by Ryall et al. [37,38] that included 107 species interacting through 207 reactions representing the various intracellular hypertrophic pathways. However, since the Ryall model did not include pregnancy hormones, and since limited experimental data on the effect of P4 on cardiomyocyte hypertrophic pathways are available [28,41], we focused on a subset of species within the original network model for which experimental data are available. Our network (Fig. 1A) consisted of 4 key inputs: the pregnancy hormones Progesterone (P4) and Estrogen (E2); Angiotensin 2 (AngII), another hormone elevated in response to both volume overload [42] and pregnancy [43]; and Stretch, a generic stimulus reflecting mechanotransduction pathways that activate Akt and MEK/ERK signaling. These inputs interacted with each other and nine other intermediate species through 24 reactions, which led to changes in cardiomyocyte size, represented by the output, CellArea.

We modeled reactions in the network using normalized Hill-type ordinary differential equations in which the level of activation of each species is represented as a normalized value between 0 and 1, where 0 indicates no signaling activity, and 1 represents maximal activation. Equation (1) shows an example of the differential equation for the intermediate species, Akt, which is activated by AngII or Stretch, but inhibited by E2 in combination with AngII activation:

$$\frac{d\text{Akt}}{dt} = \frac{1}{\tau_{\text{Akt}}}\left\{OR\left[AND\left(f_{act}(\text{AngII}), f_{inhib}(\text{E2})\right), f_{act}(\text{Stretch})\right] \cdot Y_{MAX}(\text{Akt}) - \text{Akt}\right\} \quad (1)$$

Here, τ_{Akt} is the species time constant and Y_{MAX} is the maximal fractional activation of Akt. OR and AND represent logical operations, which describe crosstalk between species:

$$OR(a,b) = a + b - a * b; AND(a,b) = a * b \quad (2)$$

The activation/inhibition functions in Equation (1) are defined such that $f_{act}(0) = 0$, $f_{act}(1) = 1$, $f_{inhib}(0) = 1$, and $f_{inhib}(1) = 0$:

$$f_{act}(X) = \frac{W \cdot BX^n}{K^n + X^n}; \; f_{inhib}(X) = W - f_{act}(X) \quad (3)$$

where W is the reaction weight, n is the Hill coefficient, and the functions B and K are defined as:

$$B = \frac{EC_{50}^n - 1}{2EC_{50}^n - 1}; K = (B-1)^{1/n} \quad (4)$$

where EC_{50} is the half-maximal activation. The MATLAB code for this model (Supplemental Document 1) was automatically generated from Supplemental Table 1 using the freely available software Netflux (https://github.com/saucermanlab/Netflux).

We simulated changing levels of hormones and stretch by adjusting the reaction weights of the inputs (W_{AngII}, W_{E2}, W_{P4}, $W_{Stretch}$) based on circulating hormone concentrations and calculated stretch as described below (Section 2.3). We set the time constant, τ, to 0.1 hours for all species except CellArea, which we set to $\tau_{\text{CellArea}} = 300$ hours to represent the longer time necessary for protein accumulation and cell growth compared to phosphorylation events. For all other parameters, we used the same default values as in Ryall et al. [37] (Table 1). We based reactions for Stretch and AngII on Ryall et al., and adjusted crosstalk interactions (AND/OR) for E2 and P4 to match phosphorylation data from *in vitro* experiments where neonatal rat ventricular cardiomyocytes were treated with P4 alone, E2 alone, AngII alone, or the combinations of P4+E2 and AngII+E2 [28,41,44–46] (Fig. 2, Supplemental Table 2).

Table 1: Signaling network model parameters

Parameter	Baseline value
Reaction weight (W)	0.1335 for inputs ($W_{Stretch}$, W_{AngII}, W_{E2}, W_{P4}) 1 for all other species
Maximal activation (Y_{max})	1
Half-maximal activation (EC_{50})	0.5
Hill coefficient (n)	1.4
Reaction time constant (τ)	0.1 hr Input and Middle Species 300 hr CellArea Output

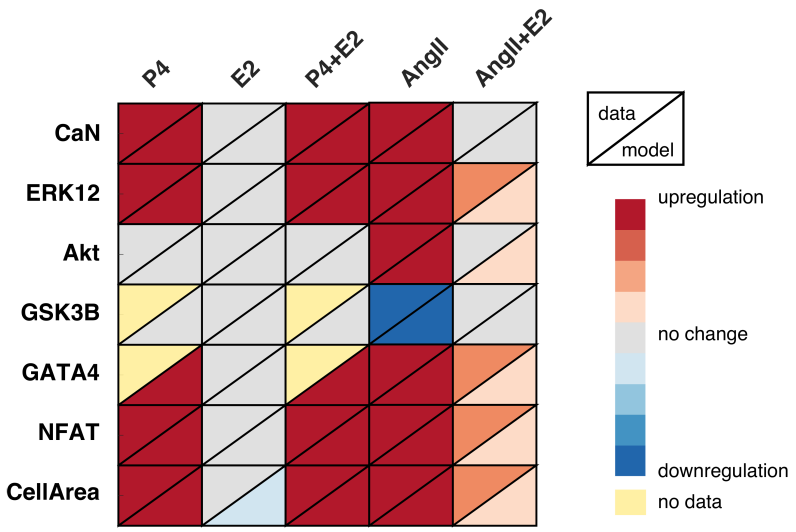

Figure 2: Intracellular signaling network model validation against *in vitro* data. Upper left triangles represent phosphorylation or activity reported from experiments where neonatal cardiomyocytes were treated with P4, E2, P4+E2, AngII, or AngII+E2 (columns). Red represents significant upregulation, grey represents no change, and blue represents downregulation of activity for each signaling intermediate (rows). Yellow color signifies no available data for a particular species and experimental condition. Lower right triangles represent network model predictions for each experimental condition. P4, E2, P4+E2 data are from [28,41]. AngII, AngII+E2 data are from [44–46]. More details are available in Supplemental Table 2.

2.2 Compartmental model of organ-level growth

Our group previously published a rapid, compartmental growth model of the heart coupled to a lumped-parameter circuit model based on a canine anatomy, and demonstrated its ability to predict heart growth in multiple settings where changes in mechanical loading of the heart occur, including volume overload (VO), pressure overload (PO), and myocardial infarction [40,47]. Briefly, this model uses a time-varying elastance model to simulate the ventricles. The end-systolic pressure-volume relationship is defined by a linear elastance and the end-diastolic pressure-volume relationship is defined by an exponential function. The systemic and pulmonary aorta and vessels are represented by capacitors in parallel with resistors, and the stressed blood volume is defined as the total blood volume contained in these capacitors and ventricles. This model is implemented as a system of differential equations in MATLAB to simulate changes in the volume of each compartment over a cardiac cycle.

2.2.1 Simulating baseline and acute volume overload hemodynamics

Because experimental studies of VO, hormonal infusion, and pregnancy are more common in small animals, we reparametrized the canine compartmental model to match control hemodynamics from rats [48,49]. To simulate volume overload in rats induced via an arteriovenous fistula between the abdominal aorta and inferior vena cava [50], we added a resistor to represent the fistula (R_{avf}) between the aorta and the vena cava (Fig. 1B). To calculate stretches experienced by the heart during baseline and acute VO states, we optimized the circulatory parameters to match averaged experimental hemodynamics reported by Holmes et al. for control rats and for rats subjected to acute VO (4 days post-fistula) [48].

We specified the reported heart rate (*HR*) and the maximum slope of the end-systolic pressure-volume relationship (*E*) directly in the model for both baseline and acute VO. We adjusted end-diastolic pressure-volume parameters (A, B, V_0) to match experimental pressures and volumes during the filling phase of the cardiac cycle. Baseline systemic resistance (R_{as}) and stressed blood volume (*SBV*) were adjusted to match the reported control values of end-systolic pressure (ESP) and end-diastolic volume (EDV). Holding the baseline R_{as} constant, the fistula resistance (R_{avf}) and *SBV* were adjusted to match experimental ESP and EDV 4 days after fistula creation. All parameters were simultaneously optimized using the fminsearch function in MATLAB, until the differences between measured and predicted hemodynamic values were minimized [40]. Figure 3 illustrates the agreement between the final calibrated baseline and acute VO model to the experimental pressure-volume behavior, and Table 2 summarizes the resulting circulation model parameters and hemodynamic comparisons between the model and data.

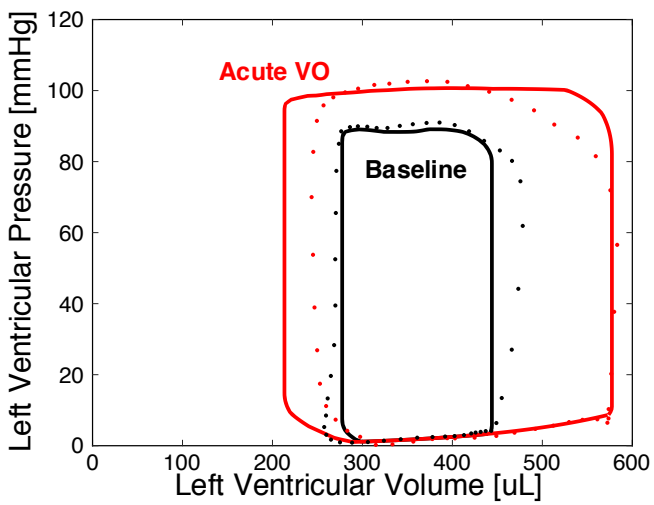

Figure 3: Pressure volume behavior for baseline and acute volume overload. Dots represent pressure-volume data points from [48] and solid lines represent model fit to the data. Black: Baseline, Red: acute volume overload.

Table 2: Circulation model parameters. Reported hemodynamic data are from [48]. ESPVR: end-systolic pressure-volume relationship and EDPVR: end-diastolic pressure-volume relationship.

	Baseline	**Volume Overload**
Specified parameters		
Heart rate (*HR*) [bpm]	373	346
Slope of the ESPVR (*E*) [mmHg/mL]	354	522
Fitted parameters		
Unloaded cavity volume (V_0) [uL]	30	
Linear term of the EDPVR (*A*) [mmHg]	0.2097	
Exponential term of the EDPVR (*B*) [1/mL]	6.90	
Systemic Resistance (R_{as}) [mmHg·s/mL]	83.71	
Arteriovenous fistula resistance (R_{avf}) [mmHg·s/mL]	Inf	75.15
Stressed blood volume (*SBV*) [uL]	3990	5380
Fitted Hemodynamic Measures		
Reported End-systolic pressure (ESP) [mmHg]	88+/-8	96+/-9
Model End-systolic pressure (ESP) [mmHg]	88	96
Reported End-diastolic volume (EDV) [uL]	445+/-75	570+/-95

Model End-diastolic volume (EDV) [uL]	444	577
Independent Hemodynamic Measures		
Reported End-systolic volume (ESV) [uL]	271+/-63	244+/-60
Model End-systolic volume (ESV) [uL]	278	213
Reported End-diastolic pressure (EDP) [mmHg]	4.49+/-0.51	6.69+/-1.10
Model End-diastolic pressure (EDP) [mHg]	5.42	10.9

2.2.2 Implementing growth in the compartmental model

We used a kinematic growth framework [51] within the compartmental model to simulate LV growth using previously published methods [40]. In this framework, the observed total stretch (F_{tot}) is a product of the growth stretch (F_g) and the elastic stretch (F_e):

$$F_{tot} = F_e \cdot F_g \quad (5)$$

where F_g is a diagonal tensor. The components of F_g were calculated based on the network model CellArea output as described in Section 2.3 below. We modeled the LV as a thin-walled spherical pressure vessel with an initial unloaded cavity volume (V_0), radius (r_0), and thickness (h_0). At each growth step, the growth tensor (F_g) was applied to update the unloaded dimensions while assuming no changes in the intrinsic material properties of the myocardium. These dimensions were then used to calculate growth-induced changes in the LV compartmental parameters. After applying growth, multiple heartbeats were simulated until a steady state was reached (compartmental volumes at the beginning and end of the cardiac cycle differed by <0.001ml). Total fiber stretch was calculated throughout the cardiac cycle based on the total chamber dimensions, then divided by the growth stretch to obtain the elastic fiber stretch:

$$F_{e,f}^{i} = \frac{r}{r_0 F_{g,f}^{i}} \quad (6)$$

where r is the deformed radius of the LV.

2.3 Multiscale cardiac growth model

The multiscale cardiac growth model (Fig. 1) was built by coupling the signaling network model of cell-level growth (Section 2.1) to the organ-level compartmental growth model (Section 2.2). To couple the two models together, we used a linear transfer function to map the elastic stretch calculated by the compartmental model (Eq. 10) to the network Stretch input, and a separate transfer function to map the network CellArea output into a growth stretch (F_g). Because the network model can only incorporate a singular, normalized input weight for Stretch, we chose to map the maximum elastic fiber stretch during a cardiac cycle, max($F_{e,f}$). We based this choice on previously published mechanics-based growth models that were successful in predicting growth in response to volume overload using the same mechanical stimulus [39,40,52]. Circulating hormone concentrations (c_{AngII}, c_{E2}, c_{P4}) were mapped to their respective network input weights using separate linear transfer functions:

$$W_{stretch} = m_{\text{stretch}} \cdot \max(F_{e,f}) + b_{\text{stretch}} \quad (7)$$

$$W_{AngII} = \mathrm{m}_{\text{AngII}} \cdot c_{AngII} + b_{AngII} \quad (8)$$

$$W_{E2} = m_{E2} \cdot c_{E2} + b_{E2} \quad (9)$$

$$W_{P4} = m_{P4} \cdot c_{P4} + b_{P4} \quad (10)$$

To translate the growth predicted by network model into a growth stretch for the compartmental model, we used a linear transfer function to map the network output, CellArea, to the determinant of the growth stretch, $J_g = \det(F_g)$. The parameters for this transfer function were set such that a half-maximal CellArea = 0.5 corresponded to no growth ($J_g = 1$) and the maximum CellArea = 1 corresponded to a doubling in mass ($J_g = 2$):

$$J_g = 2 \cdot CellArea \qquad (11)$$

Because heart growth during pregnancy results in both cavity dilation and wall thickening [4], we assumed isotropic growth such that the total increase in mass (J_g) was evenly distributed in the fiber (f), crossfiber (c), and radial (r) directions. Accordingly, the components of F_g were calculated as:

$$F_g = \begin{bmatrix} F_{g,f} & 0 & 0 \\ 0 & F_{g,c} & 0 \\ 0 & 0 & F_{g,r} \end{bmatrix} = \begin{bmatrix} J_g^{1/3} & 0 & 0 \\ 0 & J_g^{1/3} & 0 \\ 0 & 0 & J_g^{1/3} \end{bmatrix} \qquad (12)$$

2.3.1 Calibrating the multiscale model: VO, AngII, E2, P4

To calibrate the multiscale model, we optimized the unknown parameters of the linear transfer functions (Eqs. 7-10, Fig. 4) for Stretch (m_{stretch}, b_{stretch}), AngII (m_{AngII}, b_{AngII}), E2 (m_{E2}, b_{E2}), and P4 (m_{P4}, b_{P4}) to match reported LV growth from studies of experimental VO and infusion of AngII, E2, and P4. In the network model, a normalized input weight of $W_{Stretch} = W_{AngII} = W_{E2} = W_{P4} = 0.1335$ produces a steady-state CellArea = 0.5. Thus, $\max(F_{e,f})$ from the baseline compartmental model, c_{AngII} from a control male rat [42], and c_{E2} [53] and c_{P4} [54] from an ovariectomized female rat were mapped to $W_{Stretch}$, W_{AngII}, W_{E2}, and W_{P4} values of 0.1335 respectively. Accordingly, the baseline condition in our model represents a nonpregnant ovariectomized female rat or a normal male rat. To obtain a second point for calibration for each input, we simulated VO and hormonal infusion studies as described in Sections 2.3.2 and 2.3.3 below (Fig. 4).

During each growth step, $\max(F_{e,f})$ calculated from a steady state heartbeat by the compartmental model was input into the network model Stretch, The network model then ran for 5 hours of simulated time to predict changes in CellArea. Using Equations (11-12) to calculate F_g, growth was applied in the compartmental model before moving to the next growth step. Since previous studies suggest similar growth between ovariectomized female and male rats [34,35] and because studies using ovariectomized female rats are limited, we calibrated our model to growth data from ovariectomized females and male rats with the exception of P4, where only data from non-ovariectomized female mice were available [28]. For all growth simulations (Table 3), we simulated 21 days of growth based on the rat gestation period.

Because VO induces changes in AngII levels [42], we calibrated the linear transfer functions for Stretch (Eq. 7, Fig. 4A) and AngII (Eq. 8, Fig. 4B) simultaneously using reported relative changes in LV mass from VO [29,42,48,55–60] and AngII infusion [19–26] experiments in rats. To simulate VO, we set the circulatory parameters to the fitted acute VO values and maintained them throughout growth. Simultaneously, we adjusted c_{AngII} to match reported values [42] while keeping baseline c_{E2} and c_{P4}. To simulate experimental AngII infusion, we induced a

step increase in c_{AngII} while holding baseline c_{E2} and c_{P4}. In order to capture the fact that *in vivo* AngII infusion gradually increases blood pressure [20,61–63], we linearly increased the arterial resistance (R_{as}) by 3-fold over 21 days of growth.

After calibrating the Stretch and AngII inputs, we simulated LV growth due to E2 [53,64–66] and P4 [28] separately to calibrate Equations (9) and (10) (Fig. 4C,D). Similar to the AngII simulation, we induced a step increase in c_{E2} and c_{P4} while maintaining circulation parameters at baseline. In our review of the literature, we found a wide range in the reported concentrations of E2 and P4. Since no single study reported circulating E2 and P4 concentrations for ovariectomized, E2 or P4 treated, and pregnant animals, we assumed that the infusion experiments induced E2 and P4 concentrations mid-way between nonpregnant and peak pregnant levels.

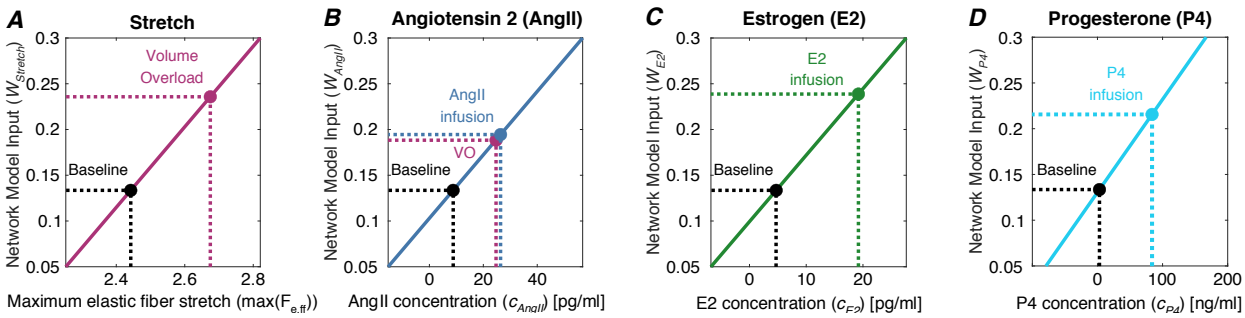

Figure 4: Linear transfer functions for network model inputs. Lines represents the linear transfer functions for the network model inputs A.) Stretch, Eq. (7), B.) Angiotensin 2, Eq. (8), C.) Estrogen, Eq. (9), and D.) Progesterone, Eq. (10). Horizontal axes represent stretch calculated by the compartmental model or hormone concentrations. Black dots represent the mapping between baseline stretch/hormones to the normalized network input, and colored dots represent the elevated stretch/hormones due to volume overload or hormone infusion used to calibrate functions.

2.3.2 Validating the multiscale model: VO+E2 and AngII+E2

After calibrating the multiscale model, we validated its ability to capture interactions between inputs. Because *in vivo* experimental heart growth data were only available for the combinations of VO+E2 [29] and AngII+E2 [44], we validated our model predictions for these two combinations. To simulate VO+E2, we implemented the same conditions as VO (described above) with an additional step increase in E2. To simulate AngII+E2, we implemented a set increase in AngII and E2, but without an increase in R_{as}, since blood pressures did not increase experimentally in mice treated with AngII+E2 [44] (Table 3).

2.3.3 Predicting heart growth during pregnancy

After calibrating and validating the multiscale model, we simulated heart growth during pregnancy by incorporating reported changes in hormones and hemodynamics. For the hormonal inputs, we implemented reported changes in c_{E2} [67], c_{P4} [68], and c_{AngII} [43] from Sprague-Dawley rats during pregnancy: E2 increases slightly in early pregnancy and reaches a peak during late pregnancy, P4 increases in early pregnancy and continues to rise and peaks in late pregnancy before suddenly dropping before delivery, and AngII increases towards the end of pregnancy. Starting in early pregnancy (by gestation day 8 of 21 in rats), cardiac output increases while mean arterial pressure (MAP) remains constant, indicating an overall decrease in systemic resistance (R_{as}). To simulate this decrease in R_{as}, we specified heart rate (HR) and calculated changes in R_{as} from the reported MAP, stroke volume (SV), and HR as $R_{as} = \mathrm{MAP}/(\mathrm{SV} \cdot HR)$ [69,70]. Total blood

volume also increases during pregnancy due to an increase in both plasma volume and red blood cells [71]. To simulate this blood volume increase during pregnancy [2,71], we allowed *SBV* to change at each growth step to match the reported time course of MAP during pregnancy (Table 3).

2.3.4 Uncertainty analysis

Finally, to understand how variability in experimental measurements affect our model predictions, we conducted uncertainty analyses for the two primary drivers of growth in the model during pregnancy, P4 and hemodynamics. First, to test how uncertainty in P4 measurements affect model predictions, we simulated a high P4 time course by implementing hormone levels at mean plus one standard deviation of the experimental data, and a low time course of P4 at the experimental mean minus 1 SD. Next, to test how uncertainty in hemodynamic measurements affect predictions, we simulated combinations of high/low MAP, high/low SV, and high/low *HR*. For these simulations, we allowed for *SBV* compensation at every growth step to match the prescribed MAP.

Table 3: Summary of growth simulations

	Simulations	Network Model Inputs				Circulation Model Parameters			Multiscale Model Output
		Stretch	AngII	E2	P4	Ras	Ravf	SBV	LV Mass
Calibration	Volume Overload (VO)	↑ [48,55,56,72]	↑ [42]			↔ [73]	↓[48]	↑[48]	↑↑ [29,42,48,55–60]
	Angiotensin 2 (AngII)		↑ [19]			↑ [20–23,61–63]			↑↑ [19–26]
	Estrogen (E2)		↔ [74]	↑ [53,75,76]		↔ [53]			↔ [53,64–66]
	Progesterone (P4)				↑ [28]*	↔ [28,77]*			↑ [28]*
Validation	VO+E2	↑		↑			↓		↑ [29]
	AngII+E2		↑	↑		↔ [44]			↔ [27,44]*
Prediction	Pregnancy	↑ [78,79]	↑ [43]	↑ [67]	↑ [68]	↓ [69,70,80]		↑	↑↑ [78,79,81,82]

3. Results

3.1 Calibrating the model: Multiscale model captures both growth and hemodynamics due to VO, AngII, E2, and P4

We were able to quantitatively capture the reported relative changes in LV mass due to experimental VO and infusion of the hormones, AngII, E2, and P4 by optimizing the linear transfer function parameters in Equations (7)-(10) (Fig. 5A, Table 3). Experimental VO and infusion with AngII in rats led to similar amounts of growth at 21 days, with LV mass increasing 30% for VO [29,42,48,55–60] and 25% for AngII [19–26]. P4 infusion led to less growth, increasing LV mass by 13%, which was reported to be significant in the experiment [28]. E2 infusion led to a small, non-significant atrophy [53,64–66] with a 5% decrease in LV mass. In addition to matching growth data, the circulatory model changes induced (Table 3) resulted in good agreement with the reported hemodynamic data with early VO [48,58,73] and AngII [20,61–63], including a step increase in cardiac output (CO) with VO and a gradual decrease in CO with AngII infusion (Fig. 5B). No changes in CO occurred in the E2 and P4 simulations, which agreed with previously reported experimental observations in mice [28,83]. Real-world and calibrated network inputs for hormone levels and stretch throughout these simulations are shown in Figure 6. Notably, the Stretch input

increased acutely and gradually decreased in our VO simulations while it remained relatively constant near baseline for AngII, E2, and P4.

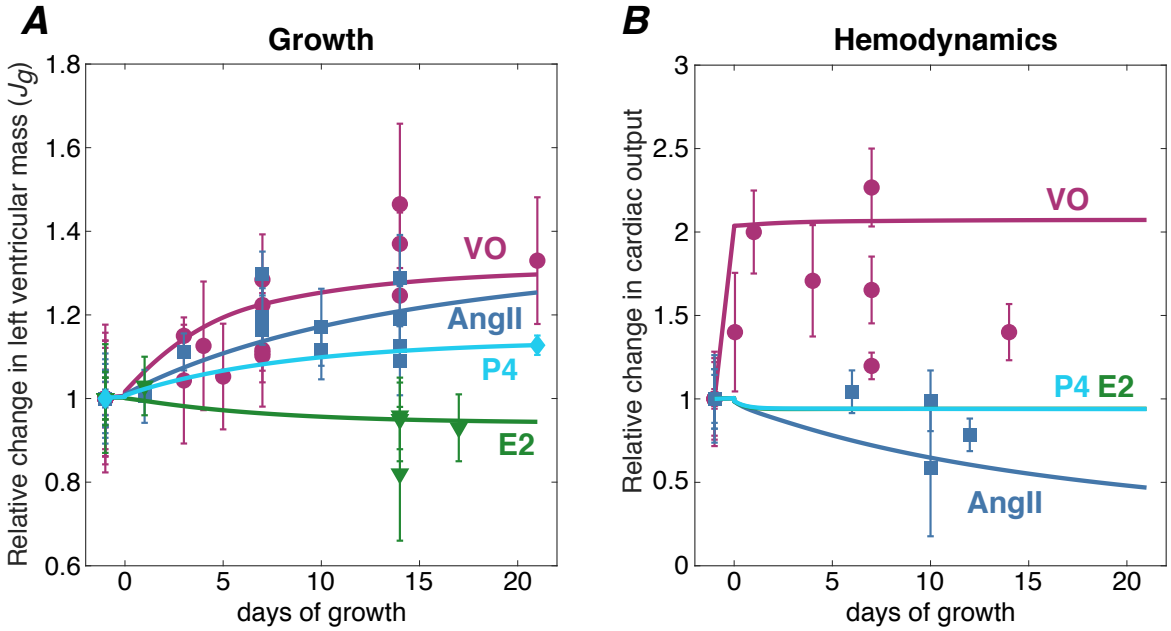

Figure 5: Calibrating the multiscale model. Model match to experimental data for volume overload (VO) [29,42,48,55–60] and Angiotensin 2 (AngII) infusion [19–26], Progesterone (P4) infusion [28], and Estrogen (E2) infusion [53,64–66]. A.) Growth quantified as relative change in left ventricular mass and B.) Hemodynamics quantified as relative change in cardiac output for VO [48,58,73], AngII [20,61–63], E2, and P4. Symbols represent reported data (see Table 3) and lines represent model fit to data. More details are available in Supplemental Table 2. (Online version in color).

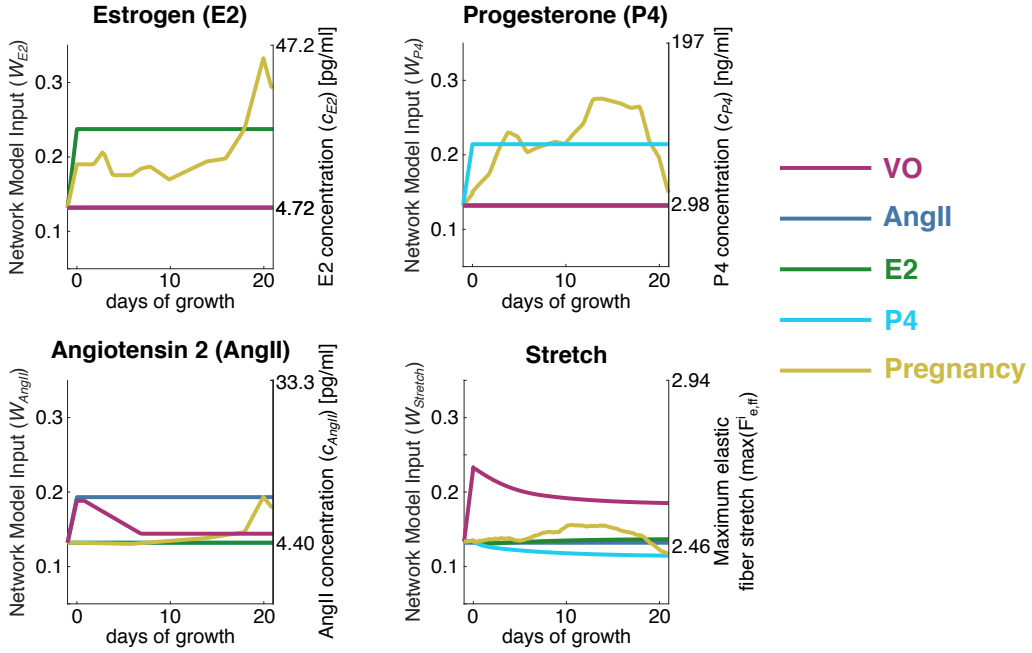

Figure 6: Calibrated hormone and stretch inputs to network model during simulated volume overload (VO), angiotensin 2 (AngII), estrogen (E2), progesterone (P4), and pregnancy simulations. Right axes show hormone concentrations in (pg/mL) or (ng/ml) and maximum elastic fiber stretch from the compartmental model. Left axes show calibrated, normalized network inputs calculated from Equations (7)-(10) (Online version in color).

3.2 Multiscale model correctly predicts attenuated growth trends with VO+E2 and AngII+E2

When we simulated the combinations of VO+E2 and AngII+E2, the model correctly predicted attenuated growth compared to VO and AngII alone (Fig. 7A,B). Furthermore, AngII+E2 led to more attenuation (12% attenuation in LV mass compared to AngII alone) compared to VO+E2 (4% attenuation in LV mass compared to VO alone), in agreement with experimental observations. In experimental VO+E2, ovariectomized rats with VO+E2 exhibited slight attenuation in growth with reported 5% LV mass attenuation at 5 days and 18% attenuation at 8 weeks [29] compared to ovariectomized rats subjected to VO alone. Conversely, ovariectomized mice treated with AngII+E2 exhibited significant attenuation in growth with reported 65% LV mass attenuation compared to AngII alone after 21 days of treatment [44]. For both cases, the model underestimated the amount of attenuation in part due to greater growth in the non-E2 animals in these specific studies compared to our calibrated model. We note that the VO+E2 study employed VO of much longer duration than our calibration studies, while the AngII+E2 study used mice rather than rats. In our AngII and AngII+E2 multiscale simulations, we observed similar activations for CaN, Akt, and GSK3B as our *in vitro* simulations (Fig. 2). This result was in agreement with the reported similar activity of CaN, Akt, and GSK3B between *in vitro* cell culture experiments and *in vivo* animal experiments [27,44].

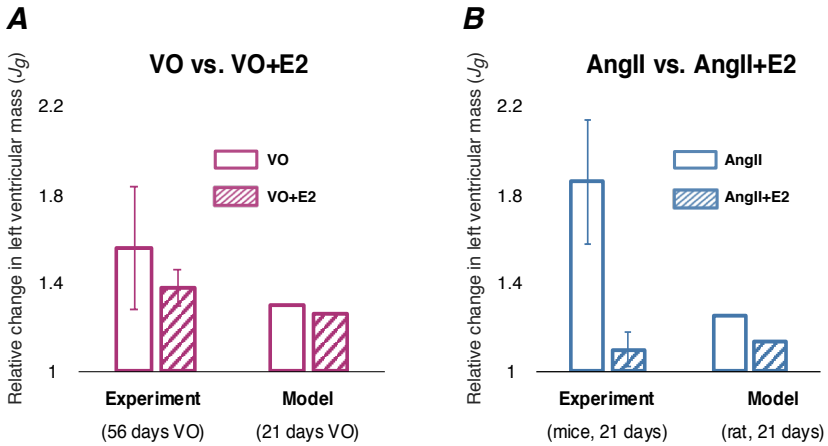

Figure 7: Validating the multiscale model. Simulations of VO+E2 and AngII+E2 (shown in dashed lines) both led to attenuated growth compared to VO only and AngII only. A.) Comparisons between experimental VO and VO+E2 at 56 days in rats [29] versus model (21 days of VO). B.) Comparisons between experimental AngII and AngII+E2 at 21 days in mice [44] versus model (21 days of simulated AngII infusion in rats).

3.3 Multiscale model predicts realistic changes in growth and hemodynamics during pregnancy

When we incorporated pregnancy hormones and circulation parameter changes, our calibrated and validated multiscale model was able to predict growth and hemodynamic changes that were in good agreement with the experimental data. Over 21 days of pregnancy, LV mass gradually increased by approximately 19% (Fig. 8A). These model predictions were within the

reported data range [78,79,81,82], except during early pregnancy where the model slightly overpredicted growth. The model slightly underpredicted the reported change in end-diastolic diameter (Fig. 8B) [78,79]. By allowing for *SBV* compensation to match the reported change in MAP (Fig. 8C) [69,70,80], we were able to match the reported gradual increase in CO (Fig. 8D) [69,70,84]. Overall, our model predicted a 14% increase in *SBV* at day 14 of pregnancy before decreasing towards the end of pregnancy (model predictions not shown).

When we examined the predicted network response for the pregnancy simulation, cell-level growth was driven primarily by species downstream of P4 (Fig. 9). Surprisingly, the network Stretch input did not change significantly, leading to no changes in the downstream signaling pathways (Akt, GSK3B, p70s6k). In our model, the elastic stretch, and therefore the network Stretch input, is dependent on the rate at which the LV volume increases versus the rate at which the ventricle grows. In our simulation, the LV growth driven by high P4 levels in early pregnancy (Fig. 6) balanced the change in LV volumes, leading to minimal change in the elastic stretches. To further understand the relative contributions of P4 and Stretch on growth during pregnancy in our model, we ran additional simulations where we maintained either P4 or Stretch at baseline (W_{P4} = 0.1335 or $W_{Stretch}$ = 0.1335). When we maintained baseline P4, the model underpredicted growth from early pregnancy (Fig. 10A, dashed blue line). Meanwhile, when we maintained baseline Stretch, the simulation followed the original predictions in early pregnancy, before deviating slightly around day 5 of pregnancy (Fig. 10A, dashed purple line). Together, these results suggest that progesterone stimulation may account for much of the cardiac hypertrophy observed during pregnancy in rats, particularly during the first half of gestation.

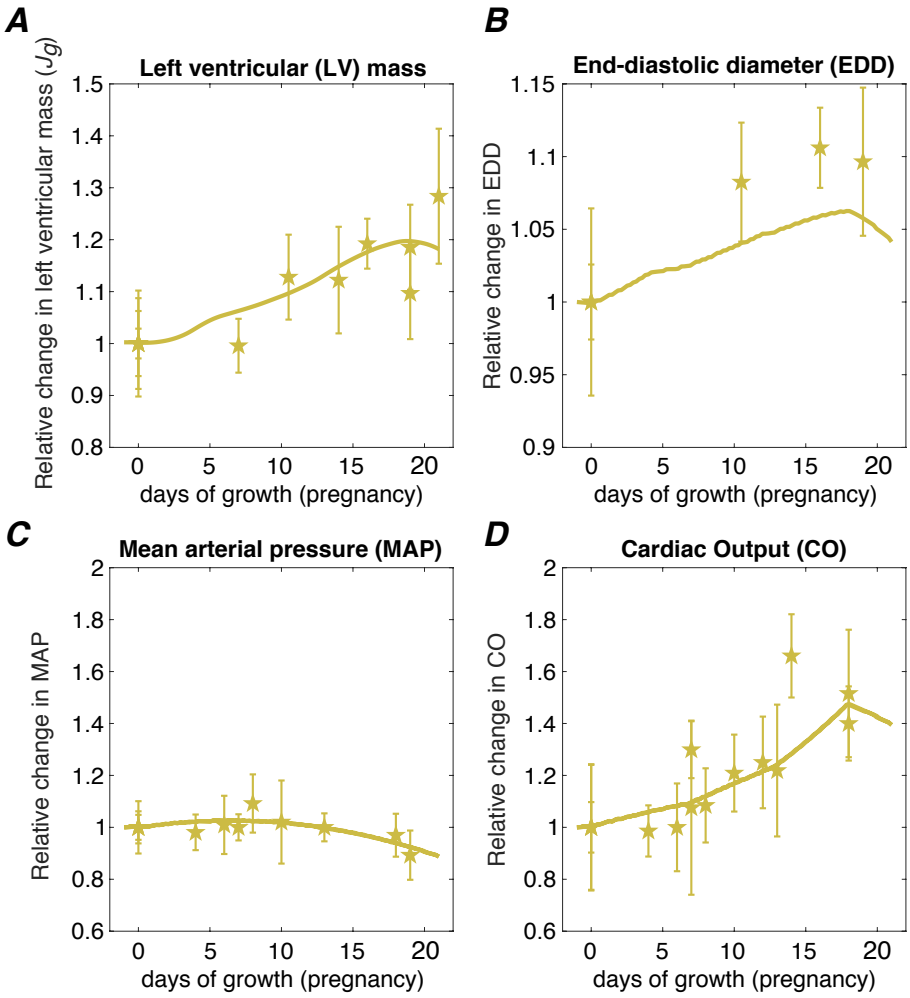

Figure 8: Multiscale model predictions for heart growth and hemodynamic changes during pregnancy. A.) Relative change in left ventricular mass, B.) Relative change in end-diastolic cavity diameter (EDD), C.) Relative change in mean arterial pressure (MAP), and D.) Relative change in mean cardiac output (CO). Symbols represent experimental data from LV mass: [78,79,81,82], EDD: [78,79], MAP: [69,70,80], CO: [69,70,84] and solid lines represent model predictions. More details are available in Supplemental Table 2.

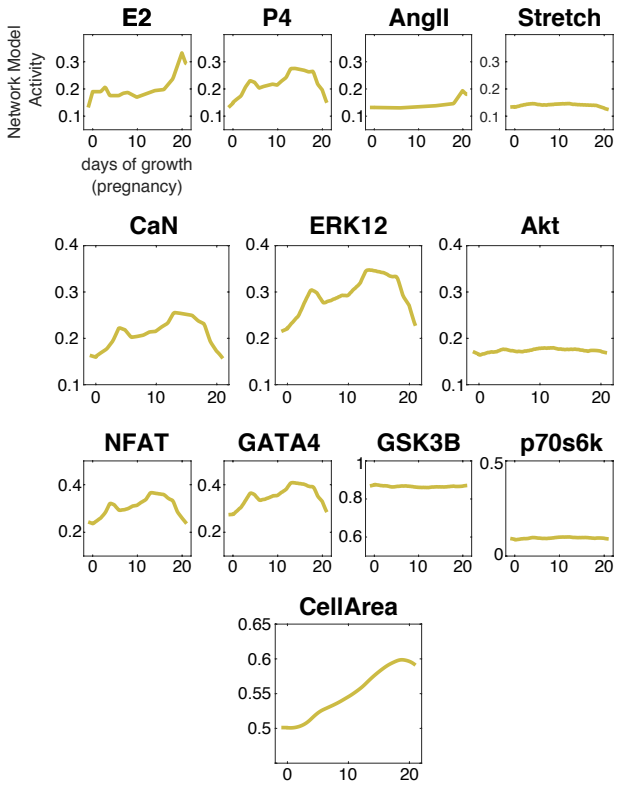

Figure 9: Activity of nodes in network model during pregnancy simulations. Each panel demonstrates changes in normalized model weights that range from 0 to 1 for a node in the signaling network (Figure 1A).

3.4 Variability in P4 and hemodynamics translate to appropriate variability in predicted growth

Finally, to investigate how uncertainty in the experimental measurements that determine inputs to our model would influence its growth predictions, we conducted additional simulations with different levels of progesterone and hemodynamics. When we repeated our pregnancy simulations with high (average plus 1 standard deviation of the reported data) and low (average minus 1 standard deviation of the reported data) levels of P4 [68], the multiscale model predicted a +/-4% LV mass change compared to our original simulations (blue area, Fig. 10B), which was slightly smaller than the standard deviation in reported LV mass at most time points. When we simulated different combinations of hemodynamic inputs for pregnancy (high/low *HR* [70], high/low SV [70], high/low MAP [69,70,80]), we observed the most growth for the combination of high SV and high MAP (+8% LV mass change) and the least growth with low SV and low MAP (-8% LV mass change) (grey area, Fig. 10C). Changing *HR* did not affect our growth predictions. These ranges of predicted growth were similar to the reported standard deviations of LV mass change. Together, these results suggest that our calibrated multiscale model provides growth predictions consistent with experimental data, with an appropriate sensitivity to known variations in the factors that drive hypertrophy during pregnancy.

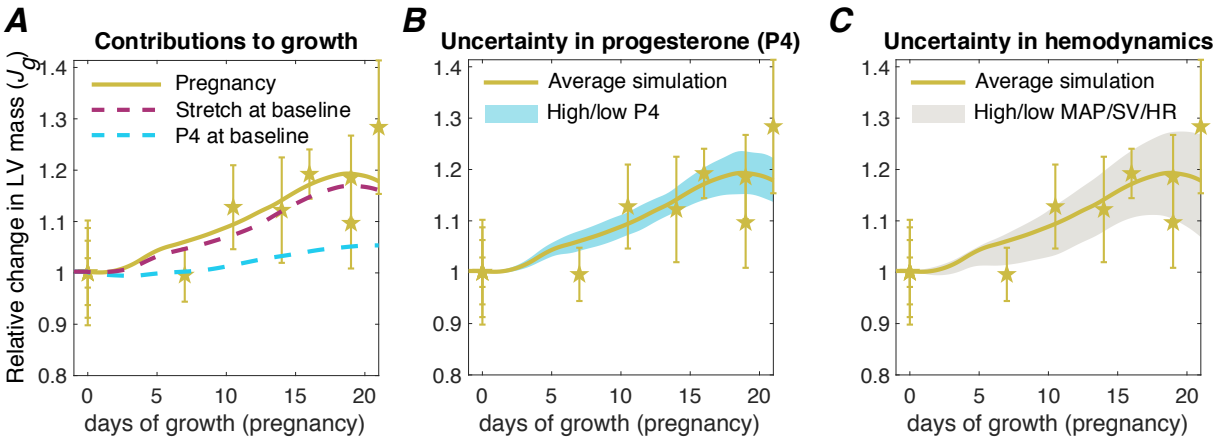

Figure 10: Effects of progesterone (P4) and hemodynamics on heart growth during pregnancy. A.) To understand the contributions of P4 and Stretch to LV growth, pregnancy simulations were repeated while maintaining P4 at baseline (dashed blue line) or Stretch at baseline (dashed purple line). To understand how the reported uncertainty in P4 and hemodynamics affect growth predictions, simulations were repeated with high and low levels of B.) P4 and C.) mean arterial pressure (MAP), stroke volume (SV), and heart rate (*HR*). Range of model predictions are represented by the shaded areas. Solid gold line represents the original pregnancy simulation with average values.

4. Discussion

The objective of this work was to develop a multiscale cardiac growth model that incorporates interactions between mechanical and hormonal signaling contributing to heart growth during pregnancy. To build this model, we coupled an intracellular signaling network model of cell-level growth to a compartmental mechanical model of organ-level growth. We first calibrated this multiscale model to heart growth in response to experimental VO and infusion experiments of AngII, E2, and P4. We then validated the model's ability to capture interactions between inputs by confirming predictions of attenuated heart growth for the combinations of VO+E2 and AngII+E2 as reported in the literature. When we simulated pregnancy by introducing appropriate changes in hormonal inputs and hemodynamics with our calibrated model, we were able to produce growth predictions that were in good agreement with experimental data. Furthermore, simulating the reported variability in progesterone concentrations and hemodynamic measures translated to appropriate variability in the predicted growth. Interestingly, the rise in progesterone that occurs during early pregnancy drove much of the LV growth in our model, resulting in minimal changes in the elastic stretch in the organ-level model, and thus the Stretch input of the network model. This result suggests that progesterone stimulation could account for much of pregnancy-induced heart growth in the rat, particularly during the early stages of pregnancy.

One striking result in this study was the constant level of Stretch throughout gestation predicted by the model (Fig. 9). In this modeling framework, changes in the elastic stretch, and therefore network model Stretch, is dependent on the rate at which LV end-diastolic volume (EDV) increases compared to the rate at which the ventricle grows. During experimental VO, a step increase in EDV occurs immediately as end-diastolic pressure (EDP) and cardiac output rise to maintain systemic flow and pressures (Table 2). Therefore, the rate of LV EDV increase clearly outpaces LV growth and the network component of the model experiences and responds to increased Stretch (Fig. 6). Conversely, in our pregnancy simulation, the rise in progesterone that

occurs in early pregnancy leads to growth that approximately matches the increase in EDV as *SBV* gradually increases throughout pregnancy. In the current implementation of the model, we chose to adjust *SBV* to match the reported MAP, which produced values of EDD (a surrogate for EDV) roughly 1 standard deviation below the reported mean values. Therefore, our pregnancy simulation may be underpredicting the degree of stretch experienced at the tissue level and therefore the contributions of Stretch-mediated pathways to heart growth during pregnancy. We therefore ran an alternate series of simulations in which we linearly increased *SBV* by 40% over 21 days of growth (Supplemental Fig. 1). This approach produced EDD values at or above the reported means and a larger increase in Stretch, similar to levels observed during our VO simulations. This version of the model overpredicted LV mass changes relative to reported means, but did remain within 1 standard deviation of the data. We conclude that additional experimental data – including simultaneous measurements of LV mass, EDD or EDV, and end-diastolic pressure (EDP) – would be needed in order to determine which of these two variants of our model is most consistent with experiments. In particular, while *SBV* is extremely difficult to measure directly, we have found in prior work that fitting EDP allows good estimation of *SBV* changes during multiple different types of overload [40].

One advantage of the modeling framework presented here is the ability to validate our predictions across multiple length scales, from intracellular signaling to organ-level growth. When we examined the predicted network response in our pregnancy simulations, species downstream of P4 (CaN, ERK12) increased in early pregnancy and peaked in late pregnancy, before dropping back to baseline levels by the end of the gestation (Fig. 9). These trends generally align with the reported levels of these species collected from mice and rat hearts throughout pregnancy [28,41,78,79,85]. However, the minimal changes in the signaling intermediates downstream of Stretch (Akt, GSK3B, p70s6k) (Fig. 9) disagree with some published data. With respect to Akt, some studies have reported an increase during pregnancy in mice and rats [41,79,86], one study reported a decrease towards late pregnancy in rats [78], and another study reported no change during late pregnancy in mice [85]. GSK3B and p70s6k have been reported to rise during mid-pregnancy before decreasing to nonpregnant levels by late gestation in mice [41]. In one in vitro study, P4 did not affect Akt phosphorylation [41], while the effect of P4 on GSK3B and p70s6k activity are unknown. To improve our predictions at the network level, there is a need for more experimental data. In particular, a better understanding of how P4 and Stretch interact is necessary. For example, an *in vivo* experiment where VO is induced along with P4 infusion could provide valuable insights into how Stretch and P4 interact to affect heart growth as well as intracellular signaling through Akt, GSK3B, and p70s6k.

In terms of the clinical applicability of this model, there are both similarities and differences between rat and human pregnancy. Generally, hemodynamic changes are similar between rats [54,69,70] and humans [1] (increase in CO, decrease in systemic resistance, and an increase in blood volume). In terms of heart growth, similar amounts of growth have been reported for rats [78,79,81,82] and human pregnancies [4], both in terms of the magnitude and patterns of growth. Hormonal profiles during pregnancy, however, differ slightly between rats and humans in that pregnant women do not exhibit a drop in progesterone before delivery [3]. Finally, another big difference between rat and human pregnancy is the average litter size. Rats generally give birth to an average litter of 11-12 pups, while most human pregnancies are singleton pregnancies. Interestingly, CO is known to be higher in patients carrying twins [1]. Before translating this model for human pregnancy, these differences should be further investigated and accounted for.

One limitation of this work is the simplified network model, where we represent a limited number of the many intracellular pathways that can lead to cardiomyocyte growth. As mentioned previously, we chose this simplified network model because experimental data on the effects of E2 and P4 on hypertrophic pathways are currently limited. As more data on how pregnancy hormones affect intracellular hypertrophic pathways become available, an exciting future direction would be to incorporate E2 and P4 into a more comprehensive network model of hypertrophy. The use of a simplified network may also explain why our model captured the trend of attenuated hypertrophy with E2 administration but underpredicted its magnitude (Fig. 7). Here again, more data are needed to allow apples-to-apples comparisons, since the studies we found that administered E2 during VO or AngII differed significantly from other studies used to tune the model in their degree of baseline hypertrophy in the absence of E2. Another limitation of this model is that we assumed isotropic growth without considering directional growth and shape changes (myocyte thickening leading to wall thickening versus myocyte lengthening leading to cavity dilation). Since pregnancy is associated with isotropic growth and because signaling pathways and mechanical signals that control these patterns of myocyte hypertrophy are currently unknown [87], we focused on matching LV mass change for our simulations. As these mechanisms become clearer, the next iteration of the model could be extended to distinguish between myocyte thickening and lengthening. Finally, when simulating hemodynamic changes during pregnancy, we implemented the reported changes in the systemic resistance without accounting for the direct effects of E2 and P4 on the aorta and vessels.

In summary, we present here a computational model of maternal heart growth during pregnancy that considers both hormonal and mechanical stimuli. In this modeling study, we calibrated the model to contributions of hormones and stretch on heart growth and demonstrated its ability to predict realistic cardiac hypertrophy during pregnancy. Furthermore, our analysis suggested that the early rise in progesterone that occurs during pregnancy may account for much of the observed heart growth in rats, particularly during the first half of gestation. Based on our model analysis, we conclude with suggestions for future experimental studies, including more cell-levels studies on the effects of pregnancy hormones on hypertrophic pathways, as well as potential *in vivo* experiments to determine the synergistic effects of elevated stretch and progesterone on heart growth.

Disclosures

None

Bibliography

[1] S. Hunter, S.C. Robson, Adaptation of the maternal heart in pregnancy, British Heart Journal. 68 (1992) 540–543. https://doi.org/10.1136/hrt.68.12.540.

[2] J.A. Pritchard, Changes in the Blood Volume During Pregnancy and Delivery, Anesthesiology. 26 (1965) 393–399. https://doi.org/10.1097/00000542-196507000-00004.

[3] D. Tulchinsky, C.J. Hobel, E. Yeager, J.R. Marshall, Plasma estrone, estradiol, estriol, progesterone, and 17-hydroxyprogesterone in human pregnancy. I. Normal pregnancy, American Journal of Obstetrics and Gynecology. 112 (1972) 1095–1100. https://doi.org/10.1016/0002-9378(72)90185-8.

[4] O. Savu, R. Jurcuţ, S. Giuşcă, T. Van Mieghem, I. Gussi, B.A. Popescu, C. Ginghină, F. Rademakers, J. Deprest, J.U. Voigt, Morphological and functional adaptation of the maternal

heart during pregnancy, Circulation: Cardiovascular Imaging. 5 (2012) 289–297. https://doi.org/10.1161/CIRCIMAGING.111.970012.
[5] A.A. Creanga, C. Syverson, K. Seed, W.M. Callaghan, Pregnancy-Related Mortality in the United States, 2011–2013, Obstetrics & Gynecology. 130 (2017) 366–373. https://doi.org/10.1097/AOG.0000000000002114.
[6] N.J. Kassebaum, R.M. Barber, Z.A. Bhutta, L. Dandona, P.W. Gething, S.I. Hay, Y. Kinfu, H.J. Larson, X. Liang, S.S. Lim, A.D. Lopez, R. Lozano, G.A. Mensah, A.H. Mokdad, M. Naghavi, C. Pinho, J.A. Salomon, C. Steiner, T. Vos, H. Wang, A.A. Abajobir, K.H. Abate, K.M. Abbas, F. Abd-Allah, M.A. Abdallat, A.M. Abdulle, S.F. Abera, V. Aboyans, I. Abubakar, N.M.E. Abu-Rmeileh, T. Achoki, A.O. Adebiyi, I.A. Adedeji, A.L. Adelekan, A.K. Adou, K.A. Afanvi, A. Agarwal, A.A. Kiadaliri, O.N. Ajala, T.F. Akinyemiju, N. Akseer, Z. Al-Aly, K. Alam, N.K.M. Alam, D. Alasfoor, S.F. Aldhahri, R.W. Aldridge, S. Alhabib, R. Ali, A. Alkerwi, F. Alla, R. Al-Raddadi, U. Alsharif, E.A. Martin, N. Alvis-Guzman, A.T. Amare, A. Amberbir, A.K. Amegah, W. Ammar, S.M. Amrock, H.H. Andersen, G.M. Anderson, R.M. Antoine, C.A.T. Antonio, A.F. Aregay, J. Ärnlöv, M. Arora, V.S.A. Arsenijevic, A. Artaman, H. Asayesh, S. Atique, E.F.G.A. Avokpaho, A. Awasthi, B.P.A. Quintanilla, P. Azzopardi, U. Bacha, A. Badawi, M.C. Bahit, K. Balakrishnan, A. Banerjee, A. Barac, S.L. Barker-Collo, T. Bärnighausen, S. Basu, T.A. Bayou, Y.T. Bayou, S. Bazargan-Hejazi, J. Beardsley, N.H. Wang, Bedi, T. Bekele, M.L. Bell, D.A. Bennett, I.M. Bensenor, A. Berhane, E. Bernabé, B.D. Betsu, A.S. Beyene, S. Biadgilign, B. Bikbov, A.A.B. Abdulhak, B.J. Biroscak, S. Biryukov, D. Bisanzio, E. Bjertness, J.D. Blore, M. Brainin, A. Brazinova, N.J.K. Breitborde, T.S. Brugha, Z.A. Butt, I.R. Campos-Nonato, J.C. Campuzano, R. Cárdenas, J.J. Carrero, A. Carter, D.C. Casey, C.A. Castañeda-Orjuela, R.E. Castro, F. Catalá-López, F. Cavalleri, H.-Y. Chang, J.-C. Chang, L. Chavan, C.E. Chibueze, V.H. Chisumpa, J.-Y.J. Choi, R. Chowdhury, D.J. Christopher, L.G. Ciobanu, M. Cirillo, M.M. Coates, M. Coggeshall, V. Colistro, S.M. Colquhoun, C. Cooper, L.T. Cooper, M. Cortinovis, T. Dahiru, A. Damasceno, H. Danawi, R. Dandona, J. das Neves, D.D. Leo, R.P. Dellavalle, K. Deribe, A. Deribew, D.C. Des Jarlais, S.D. Dharmaratne, D.J. Dicker, E.L. Ding, E. Dossou, M. Dubey, B.E. Ebel, C.L. Ellingsen, I. Elyazar, A.Y. Endries, S.P. Ermakov, B. Eshrati, A. Esteghamati, E.J.A. Faraon, T.A. Farid, C.S. e S. Farinha, A. Faro, M.S. Farvid, F. Farzadfar, S.-M. Fereshtehnejad, J.C. Fernandes, F. Fischer, J.R.A. Fitchett, T. Fleming, N. Foigt, E.B. Franca, R.C. Franklin, M.S. Fraser, J. Friedman, N. Fullman, T. Fürst, N.D. Futran, K. Gambashidze, A. Gamkrelidze, T. Gebre, T.T. Gebrehiwot, A.T. Gebremedhin, M. Gebremedhin, A.A. Gebru, J.M. Geleijnse, K.B. Gibney, A.Z. Giref, M. Giroud, M.D. Gishu, E. Glaser, S. Goenka, H. Gomez-Dantes, P. Gona, A. Goodridge, S.V. Gopalani, A. Goto, N. Graetz, H.C. Gugnani, Y. Guo, R. Gupta, R. Gupta, V. Gupta, N. Hafezi-Nejad, A.D. Hailu, G.B. Hailu, R.R. Hamadeh, S. Hamidi, J. Hancock, A.J. Handal, G.J. Hankey, H.L. Harb, S. Harikrishnan, K.M. Harun, R. Havmoeller, H.W. Hoek, M. Horino, N. Horita, H.D. Hosgood, D.G. Hoy, A.S. Htet, G. Hu, H. Huang, J.J. Huang, I. Huybrechts, C. Huynh, M. Iannarone, K.M. Iburg, B.T. Idrisov, V.J. Iyer, K.H. Jacobsen, N. Jahanmehr, M.B. Jakovljevic, M. Javanbakht, A.U. Jayatilleke, S.H. Jee, P. Jeemon, V. Jha, G. Jiang, Y. Jiang, T. Jibat, J.B. Jonas, Z. Kabir, R. Kamal, H. Kan, A. Karch, D. Karletsos, A. Kasaeian, A. Kaul, N. Kawakami, J.F. Kayibanda, K. Kazanjan, D.S. Kazi, P.N. Keiyoro, L. Kemmer, A.H. Kemp, A.P. Kengne, A. Keren, M. Kereselidze, C.N. Kesavachandran, Y.S. Khader, A.R. Khan, E.A. Khan, Y.-H. Khang, I. Khonelidze, A. Khosravi, J. Khubchandani, Y.J. Kim, M. Kivipelto, L.D. Knibbs, Y. Kokubo, S. Kosen,

P.A. Koul, A. Koyanagi, S. Krishnaswami, B.K. Defo, B.K. Bicer, A.A. Kudom, X.R. Kulikoff, C. Kulkarni, G.A. Kumar, M.J. Kutz, D.K. Lal, R. Lalloo, H. Lam, H. Lamadrid-Figueroa, Q. Lan, A. Larsson, D.O. Laryea, J. Leigh, R. Leung, Y. Li, Y. Li, S.E. Lipshultz, P.Y. Liu, S. Liu, Y. Liu, B.K. Lloyd, P.A. Lotufo, R. Lunevicius, S. Ma, H.M.A.E. Razek, M.M.A.E. Razek, M. Majdan, A. Majeed, R. Malekzadeh, C.C. Mapoma, W. Marcenes, D.J. Margolis, N. Marquez, F. Masiye, M.B. Marzan, A.J. Mason-Jones, T.T. Mazorodze, P.A. Meaney, A. Mehari, M.M. Mehndiratta, F. Mejia-Rodriguez, A.B. Mekonnen, Y.A. Melaku, Z.A. Memish, W. Mendoza, A. Meretoja, T.J. Meretoja, F.A. Mhimbira, T.R. Miller, E.J. Mills, M. Mirarefin, A. Misganaw, N.M. Ibrahim, K.A. Mohammad, A. Mohammadi, S. Mohammed, G.L.D. Mola, L. Monasta, J. de la Cruz Monis, J.C.M. Hernandez, P. Montero, M. Montico, M.D. Mooney, A.R. Moore, M. Moradi-Lakeh, L. Morawska, R. Mori, U.O. Mueller, G.V.S. Murthy, S. Murthy, J.B. Nachega, A. Naheed, L. Naldi, D. Nand, V. Nangia, D. Nash, S. Neupane, J.N. Newton, M. Ng, F.N. Ngalesoni, P. Nguhiu, G. Nguyen, Q.L. Nguyen, M.I. Nisar, M. Nomura, O.F. Norheim, R.E. Norman, L. Nyakarahuka, C.M. Obermeyer, F.A. Ogbo, I.-H. Oh, F.A. Ojelabi, P.R. Olivares, B.O. Olusanya, J.O. Olusanya, J.N. Opio, E. Oren, E. Ota, A.S. Oyekale, M. Pa, A. Pain, N. Papantoniou, E.-K. Park, H.-Y. Park, A.J.P. Caicedo, S.B. Patten, V.K. Paul, D.M. Pereira, N. Perico, K. Pesudovs, M. Petzold, M.R. Phillips, J.D. Pillay, F. Pishgar, S. Polinder, D. Pope, F. Pourmalek, M. Qorbani, A. Rafay, K. Rahimi, V. Rahimi-Movaghar, M. Rahman, M.H.U. Rahman, S.U. Rahman, R.K. Rai, U. Ram, C.L. Ranabhat, T. Rangaswamy, P.V. Rao, A.H. Refaat, G. Remuzzi, S. Resnikoff, D. Rojas-Rueda, L. Ronfani, G. Roshandel, A. Roy, G.M. Ruhago, R. Sagar, M.M. Saleh, J.R. Sanabria, M.D. Sanchez-Niño, I.S. Santos, J.V. Santos, R. Sarmiento-Suarez, B. Sartorius, M. Satpathy, M. Savic, M. Sawhney, M.I. Saylan, I.J.C. Schneider, D.C. Schwebel, S. Seedat, S.G. Sepanlou, E.E. Servan-Mori, T. Setegn, K.A. Shackelford, M.A. Shaikh, M. Shakh-Nazarova, R. Sharma, J. She, S. Sheikhbahaei, J. Shen, K. Shibuya, M.-J. Shin, R. Shiri, K. Shishani, I. Shiue, I.D. Sigfusdottir, N. Silpakit, D.A.S. Silva, D.G.A. Silveira, J.I. Silverberg, E.P. Simard, S. Sindi, A. Singh, J.A. Singh, O.P. Singh, P.K. Singh, V. Singh, V. Skirbekk, A. Sligar, K. Sliwa, J.M. Smith, S. Soneji, R.J.D. Sorensen, J.B. Soriano, S. Soshnikov, L.A. Sposato, C.T. Sreeramareddy, V. Stathopoulou, K. Stroumpoulis, L. Sturua, B.F. Sunguya, S. Swaminathan, B.L. Sykes, C.E.I. Szoeke, R. Tabarés-Seisdedos, K.M. Tabb, R.T. Talongwa, M. Tavakkoli, B. Taye, B.A. Tedla, W.M. Tefera, T. Tekle, G.T. Shifa, A.S. Terkawi, F.H. Tesfay, G.A. Tessema, A.J. Thomson, A.L. Thorne-Lyman, R. Tobe-Gai, R. Topor-Madry, J.A. Towbin, B.X. Tran, Z.T. Dimbuene, A.K. Tura, S. Tyrovolas, K.N. Ukwaja, O.A. Uthman, T. Vasankari, N. Venketasubramanian, F.S. Violante, S.K. Vladimirov, V.V. Vlassov, S.E. Vollset, J.A. Wagner, L. Wang, S. Weichenthal, E. Weiderpass, R.G. Weintraub, A. Werdecker, R. Westerman, T. Wijeratne, J.D. Wilkinson, C.S. Wiysonge, S.M. Woldeyohannes, C.D.A. Wolfe, T. Wolock, S. Won, M. Wubshet, Q. Xiao, G. Xu, A.K. Yadav, B. Yakob, A.Z. Yalew, Y. Yano, H.G. Yebyo, P. Yip, N. Yonemoto, S.-J. Yoon, M.Z. Younis, C. Yu, S. Yu, Z. Zaidi, M.E.S. Zaki, H. Zeeb, Y. Zhao, Y. Zhao, M. Zhou, S. Zodpey, L.J. Zuhlke, C.J.L. Murray, Global, regional, and national levels of maternal mortality, 1990–2015: a systematic analysis for the Global Burden of Disease Study 2015, The Lancet. 388 (2016) 1775–1812. https://doi.org/10.1016/S0140-6736(16)31470-2.

[7] L.J. De Windt, H.W. Lim, O.F. Bueno, Q. Liang, U. Delling, J.C. Braz, B.J. Glascock, T.F. Kimball, F. del Monte, R.J. Hajjar, J.D. Molkentin, Targeted inhibition of calcineurin

attenuates cardiac hypertrophy in vivo, Proceedings of the National Academy of Sciences. 98 (2001) 3322–3327. https://doi.org/10.1073/pnas.031371998.
[8] N. Tuerdi, L. Xu, B. Zhu, C. Chen, Y. Cao, Y. Wang, Q. Zhang, Z. Li, R. Qi, Preventive effects of simvastatin nanoliposome on isoproterenol-induced cardiac remodeling in mice, Nanomedicine: Nanotechnology, Biology and Medicine. 12 (2016) 1899–1907. https://doi.org/10.1016/j.nano.2016.05.002.
[9] M.A. Allwood, R.T. Kinobe, L. Ballantyne, N. Romanova, L.G. Melo, C.A. Ward, K.R. Brunt, J.A. Simpson, Heme oxygenase-1 overexpression exacerbates heart failure with aging and pressure overload but is protective against isoproterenol-induced cardiomyopathy in mice, Cardiovascular Pathology. 23 (2014) 231–237. https://doi.org/10.1016/j.carpath.2014.03.007.
[10] C.C. Sucharov, J.G. Hijmans, R.D. Sobus, W.F.A. Melhado, S.D. Miyamoto, B.L. Stauffer, β-Adrenergic receptor antagonism in mice: a model for pediatric heart disease, Journal of Applied Physiology. 115 (2013) 979–987. https://doi.org/10.1152/japplphysiol.00627.2013.
[11] O. Drews, O. Tsukamoto, D. Liem, J. Streicher, Y. Wang, P. Ping, Differential Regulation of Proteasome Function in Isoproterenol-Induced Cardiac Hypertrophy, Circ Res. 107 (2010) 1094–1101. https://doi.org/10.1161/CIRCRESAHA.110.222364.
[12] S. Tshori, Transcription factor MITF regulates cardiac growth and hypertrophy, Journal of Clinical Investigation. 116 (2006) 2673–2681. https://doi.org/10.1172/JCI27643.
[13] Y. Zhang, J. Xu, Z. Long, C. Wang, L. Wang, P. Sun, P. Li, T. Wang, Hydrogen (H2) Inhibits Isoproterenol-Induced Cardiac Hypertrophy via Antioxidative Pathways, Front. Pharmacol. 7 (2016). https://doi.org/10.3389/fphar.2016.00392.
[14] S.B. Waters, D.M. Diak, M. Zuckermann, P.H. Goldspink, L. Leoni, B.B. Roman, Genetic background influences adaptation to cardiac hypertrophy and Ca2+ handling gene expression, Front. Physiol. 4 (2013). https://doi.org/10.3389/fphys.2013.00011.
[15] Y. Ryu, L. Jin, H.J. Kee, Z.H. Piao, J.Y. Cho, G.R. Kim, S.Y. Choi, M.Q. Lin, M.H. Jeong, Gallic acid prevents isoproterenol-induced cardiac hypertrophy and fibrosis through regulation of JNK2 signaling and Smad3 binding activity, Sci Rep. 6 (2016) 34790. https://doi.org/10.1038/srep34790.
[16] E.J. Jaehnig, A.B. Heidt, S.B. Greene, I. Cornelissen, B.L. Black, Increased Susceptibility to Isoproterenol-Induced Cardiac Hypertrophy and Impaired Weight Gain in Mice Lacking the Histidine-Rich Calcium-Binding Protein, MCB. 26 (2006) 9315–9326. https://doi.org/10.1128/MCB.00482-06.
[17] C.L. Galindo, M.A. Skinner, M. Errami, L.D. Olson, D.A. Watson, J. Li, J.F. McCormick, L.J. McIver, N.M. Kumar, T.Q. Pham, H.R. Garner, Transcriptional profile of isoproterenol-induced cardiomyopathy and comparison to exercise-induced cardiac hypertrophy and human cardiac failure, BMC Physiol. 9 (2009) 23. https://doi.org/10.1186/1472-6793-9-23.
[18] W.W. Brooks, C.H. Conrad, Isoproterenol-Induced Myocardial Injury and Diastolic Dysfunction in Mice: Structural and Functional Correlates, Comparative Medicine. 59 (2009) 5.
[19] S.A. Griffin, W.C. Brown, F. MacPherson, J.C. McGrath, V.G. Wilson, N. Korsgaard, M.J. Mulvany, A.F. Lever, Angiotensin II causes vascular hypertrophy in part by a non-pressor mechanism., Hypertension. 17 (1991) 626–635. https://doi.org/10.1161/01.HYP.17.5.626.

[20] H. Belabbas, S. Zalvidea, D. Casellas, J.-P. Molès, O. Galbes, J. Mercier, B. Jover, Contrasting effect of exercise and angiotensin II hypertension on in vivo and in vitro cardiac angiogenesis in rats, American Journal of Physiology-Regulatory, Integrative and Comparative Physiology. 295 (2008) R1512–R1518. https://doi.org/10.1152/ajpregu.00014.2008.
[21] D.E. Dostal, K.M. Baker, Angiotensin II Stimulation of Left Ventricular Hypertrophy in Adult Rat Heart, American Journal of Hypertension. 5 (1992) 276–280. https://doi.org/10.1093/ajh/5.5.276.
[22] X. Zhang, F. Meng, J. Song, L. Zhang, J. Wang, D. Li, L. Li, P. Dong, B. Yang, Y. Chen, Pentoxifylline Ameliorates Cardiac Fibrosis, Pathological Hypertrophy, and Cardiac Dysfunction in Angiotensin II-induced Hypertensive Rats, Journal of Cardiovascular Pharmacology. 67 (2016) 76–85. https://doi.org/10.1097/FJC.0000000000000316.
[23] L. Zhang, M. Deng, A. Lu, Y. Chen, Y. Chen, C. Wu, Z. Tan, K.M. Boini, T. Yang, Q. Zhu, L. Wang, Sodium butyrate attenuates angiotensin II-induced cardiac hypertrophy by inhibiting COX2/PGE2 pathway via a HDAC5/HDAC6-dependent mechanism, J Cell Mol Med. 23 (2019) 8139–8150. https://doi.org/10.1111/jcmm.14684.
[24] R. Dilley, Heparin inhibits mesenteric vascular hypertrophy in angiotensin II-infusion hypertension in rats, Cardiovascular Research. 38 (1998) 247–255. https://doi.org/10.1016/S0008-6363(98)00004-2.
[25] S. Kim, K. Ohta, A. Hamaguchi, T. Yukimura, K. Miura, H. Iwao, Angiotensin II induces cardiac phenotypic modulation and remodeling in vivo in rats, Hypertension. 25 (1995) 1252–1259. https://doi.org/10.1161/01.hyp.25.6.1252.
[26] S. Kim-Mitsuyama, Y. Izumi, Y. Izumiya, M. Namba, K. Yoshida, R. Wake, M. Yoshiyama, H. Iwao, Dominant-negative c-Jun inhibits rat cardiac hypertrophy induced by angiotensin II and hypertension, Gene Ther. 13 (2006) 348–355. https://doi.org/10.1038/sj.gt.3302670.
[27] A. Pedram, M. Razandi, D. Lubahn, J. Liu, M. Vannan, E.R. Levin, Estrogen inhibits cardiac hypertrophy: Role of estrogen receptor-β to inhibit calcineurin, Endocrinology. 149 (2008) 3361–3369. https://doi.org/10.1210/en.2008-0133.
[28] E. Chung, F. Yeung, L.A. Leinwand, Calcineurin activity is required for cardiac remodelling in pregnancy, Cardiovascular Research. 100 (2013) 402–410. https://doi.org/10.1093/cvr/cvt208.
[29] T.G. Voloshenyuk, J.D. Gardner, Estrogen improves TIMP-MMP balance and collagen distribution in volume-overloaded hearts of ovariectomized females, American Journal of Physiology-Regulatory, Integrative and Comparative Physiology. 299 (2010) R683–R693. https://doi.org/10.1152/ajpregu.00162.2010.
[30] A. Iorga, J. Li, S. Sharma, S. Umar, J.C. Bopassa, R.D. Nadadur, A. Centala, S. Ren, T. Saito, L. Toro, Y. Wang, E. Stefani, M. Eghbali, Rescue of pressure overload-induced heart failure by estrogen therapy, Journal of the American Heart Association. 5 (2016) 1–12. https://doi.org/10.1161/JAHA.115.002482.
[31] D. Fliegner, C. Schubert, A. Penkalla, H. Witt, G. Kararigas, E. Dworatzek, E. Staub, P. Martus, P.R. Noppinger, U. Kintscher, J.-Å. Gustafsson, V. Regitz-Zagrosek, Female sex and estrogen receptor-β attenuate cardiac remodeling and apoptosis in pressure overload, American Journal of Physiology-Regulatory, Integrative and Comparative Physiology. 298 (2010) R1597–R1606. https://doi.org/10.1152/ajpregu.00825.2009.

[32] H. Tagashira, S. Bhuiyan, N. Shioda, K. Fukunaga, Distinct cardioprotective effects of 17β-estradiol and dehydroepiandrosterone on pressure overload–induced hypertrophy in ovariectomized female rats:, Menopause. 18 (2011) 1317–1326. https://doi.org/10.1097/gme.0b013e31821f915b.
[33] R.D. Patten, I. Pourati, M.J. Aronovitz, A. Alsheikh-Ali, S. Eder, T. Force, M.E. Mendelsohn, R.H. Karas, 17 Beta-Estradiol Differentially Affects Left Ventricular and Cardiomyocyte Hypertrophy Following Myocardial Infarction and Pressure Overload, Journal of Cardiac Failure. 14 (2008) 245–253. https://doi.org/10.1016/j.cardfail.2007.10.024.
[34] J.D. Gardner, G.L. Brower, J.S. Janicki, Gender differences in cardiac remodeling secondary to chronic volume overload, Journal of Cardiac Failure. 8 (2002) 101–107. https://doi.org/10.1054/jcaf.2002.32195.
[35] G.L. Brower, J.D. Gardner, J.S. Janicki, Gender mediated cardiac protection from adverse ventricular remodeling is abolished by ovariectomy, Molecular and Cellular Biochemistry. 251 (2003) 89–95. https://doi.org/10.1023/A:1025438000942.
[36] K. Yoshida, J.W. Holmes, Computational models of cardiac hypertrophy, Progress in Biophysics and Molecular Biology. (2020) S0079610720300651. https://doi.org/10.1016/j.pbiomolbio.2020.07.001.
[37] K.A. Ryall, D.O. Holland, K.A. Delaney, M.J. Kraeutler, A.J. Parker, J.J. Saucerman, Network Reconstruction and Systems Analysis of Cardiac Myocyte Hypertrophy Signaling, Journal of Biological Chemistry. 287 (2012) 42259–42268. https://doi.org/10.1074/jbc.M112.382937.
[38] D.U. Frank, M.D. Sutcliffe, J.J. Saucerman, Network-based predictions of in vivo cardiac hypertrophy, Journal of Molecular and Cellular Cardiology. 121 (2018) 180–189. https://doi.org/10.1016/j.yjmcc.2018.07.243.
[39] C.M. Witzenburg, J.W. Holmes, A comparison of phenomenologic growth laws for myocardial hypertrophy, Journal of Elasticity. 129 (2017) 257–281. https://doi.org/10.1007/s10659-017-9631-8.
[40] C.M. Witzenburg, J.W. Holmes, Predicting the time course of ventricular dilation and thickening using a rapid compartmental model, Journal of Cardiovascular Translational Research. (2018). https://doi.org/10.1007/s12265-018-9793-1.
[41] E. Chung, F. Yeung, L.A. Leinwand, Akt and MAPK signaling mediate pregnancy-induced cardiac adaptation, Journal of Applied Physiology. 112 (2012) 1564–1575. https://doi.org/10.1152/japplphysiol.00027.2012.
[42] M. Ruzicka, F.H. Leenen, Relevance of blockade of cardiac and circulatory angiotensin-converting enzyme for the prevention of volume overload-induced cardiac hypertrophy, Circulation. 91 (1995) 16–19. https://doi.org/10.1161/01.cir.91.1.16.
[43] J.S. Mishra, K. Gopalakrishnan, S. Kumar, Pregnancy upregulates angiotensin type 2 receptor expression and increases blood flow in uterine arteries of rats, Biology of Reproduction. 99 (2018) 1091–1099. https://doi.org/10.1093/biolre/ioy130.
[44] A. Pedram, M. Razandi, K.S. Korach, R. Narayanan, J.T. Dalton, E.R. Levin, ERβ selective agonist inhibits angiotensin-induced cardiovascular pathology in female mice, Endocrinology. 154 (2013) 4352–4364. https://doi.org/10.1210/en.2013-1358.
[45] A. Pedram, M. Razandi, M. Aitkenhead, E.R. Levin, Estrogen inhibits cardiomyocyte hypertrophy in vitro: Antagonism of calcineurin-related hypertrophy through induction of

MCIP1, Journal of Biological Chemistry. 280 (2005) 26339–26348. https://doi.org/10.1074/jbc.M414409200.
[46] A. Pedram, M. Razandi, R. Narayanan, J.T. Dalton, T.A. McKinsey, E.R. Levin, Estrogen regulates histone deacetylases to prevent cardiac hypertrophy, Molecular Biology of the Cell. 24 (2013) 3805–3818. https://doi.org/10.1091/mbc.E13-08-0444.
[47] W.P. Santamore, D. Burkhoff, Hemodynamic consequences of ventricular interaction as assessed by model analysis, American Journal of Physiology-Heart and Circulatory Physiology. 260 (1991) H146–H157. https://doi.org/10.1152/ajpheart.1991.260.1.H146.
[48] J.W. Holmes, Candidate mechanical stimuli for hypertrophy during volume overload, Journal of Applied Physiology. 97 (2004) 1453–1460. https://doi.org/10.1152/japplphysiol.00834.2003.
[49] C.M. Witzenburg, L.R. Caggiano, J.W. Holmes, Animal-specific hemodynamic compensation following myocardial infarction, in: Summer Biomechanics, Bioengineering, and Biotransport Conference, 2020: p. 2.
[50] R. Garcia, S. Diebold, Simple, rapid, and effective method of producing aortocaval shunts in the rat, Cardiovascular Research. 24 (1990) 430–432. https://doi.org/10.1093/cvr/24.5.430.
[51] E.K. Rodriguez, A. Hoger, A.D. McCulloch, Stress-dependent finite growth in soft elastic tissues, Journal of Biomechanics. 27 (1994) 455–467. https://doi.org/10.1016/0021-9290(94)90021-3.
[52] R.C.P. Kerckhoffs, J.H. Omens, A.D. McCulloch, A single strain-based growth law predicts concentric and eccentric cardiac growth during pressure and volume overload, Mechanics Research Communications. 42 (2012) 40–50. https://doi.org/10.1016/j.mechrescom.2011.11.004.
[53] M. Jankowski, G. Rachelska, W. Donghao, S.M. McCann, J. Gutkowska, Estrogen receptors activate atrial natriuretic peptide in the rat heart, Proceedings of the National Academy of Sciences of the United States of America. 98 (2001) 11765–11770. https://doi.org/10.1073/pnas.201394198.
[54] M.L. Blair, D. Mickelsen, Plasma protein and blood volume restitution after hemorrhage in conscious pregnant and ovarian steroid-replaced rats, American Journal of Physiology-Regulatory, Integrative and Comparative Physiology. 290 (2006) R425–R434. https://doi.org/10.1152/ajpregu.00011.2005.
[55] A.J. Mouton, V.K. Ninh, E.C. El Hajj, M.C. El Hajj, N.W. Gilpin, J.D. Gardner, Exposure to chronic alcohol accelerates development of wall stress and eccentric remodeling in rats with volume overload, Journal of Molecular and Cellular Cardiology. 97 (2016) 15–23. https://doi.org/10.1016/j.yjmcc.2016.04.010.
[56] M. Ruzicka, B. Yuan, E. Harmsen, F.H. Leenen, The renin-angiotensin system and volume overload-induced cardiac hypertrophy in rats. Effects of angiotensin converting enzyme inhibitor versus angiotensin II receptor blocker., Circulation. 87 (1993) 921–930. https://doi.org/10.1161/01.cir.87.3.921.
[57] G.L. Brower, J.R. Henegar, J.S. Janicki, Temporal evaluation of left ventricular remodeling and function in rats with chronic volume overload., The American Journal of Physiology. 271 (1996) H2071–8. https://doi.org/10.1152/ajpheart.1996.271.5.H2071.
[58] D.B. Murray, J.D. Gardner, G.L. Brower, J.S. Janicki, Effects of nonselective endothelin-1 receptor antagonism on cardiac mast cell-mediated ventricular remodeling in rats,

American Journal of Physiology-Heart and Circulatory Physiology. 294 (2008) H1251–H1257. https://doi.org/10.1152/ajpheart.00622.2007.
[59] X. Wang, B. Ren, S. Liu, E. Sentex, P.S. Tappia, N.S. Dhalla, Characterization of cardiac hypertrophy and heart failure due to volume overload in the rat, Journal of Applied Physiology. 94 (2003) 752–763. https://doi.org/10.1152/japplphysiol.00248.2002.
[60] P. Hatt, Morphometry and ultrastructure of heart hypertrophy induced by chronic volume overload (aorto-caval fistula in the rat), Journal of Molecular and Cellular Cardiology. 11 (1979) 989–998. https://doi.org/10.1016/0022-2828(79)90390-0.
[61] S. Fujioka, O. Sasakawa, H. Kishimoto, K. Tsumura, H. Morii, The antihypertensive effect of calcitonin gene-related peptide in rats with norepinephrine- and angiotensin II-induced hypertension, J. Hypertens. 9 (1991) 175–179. https://doi.org/10.1097/00004872-199102000-00013.
[62] A. Nishiyama, T. Fukui, Y. Fujisawa, M. Rahman, R.-X. Tian, S. Kimura, Y. Abe, Systemic and Regional Hemodynamic Responses to Tempol in Angiotensin II–Infused Hypertensive Rats, Hypertension. 37 (2001) 77–83. https://doi.org/10.1161/01.HYP.37.1.77.
[63] J.L. Pasquié, A. Herizi, B. Jover, A. Mimran, Chronic Bradykinin Infusion and Receptor Blockade in Angiotensin II Hypertension in Rats, Hypertension. 33 (1999) 830–834. https://doi.org/10.1161/01.HYP.33.3.830.
[64] S.H. Chu, P. Goldspink, J. Kowalski, J. Beck, D.W. Schwertz, Effect of estrogen on calcium-handling proteins, β-adrenergic receptors, and function in rat heart, Life Sciences. 79 (2006) 1257–1267. https://doi.org/10.1016/j.lfs.2006.03.037.
[65] J. Goldstein, C.K. Sites, M.J. Toth, Progesterone stimulates cardiac muscle protein synthesis via receptor-dependent pathway, Fertility and Sterility. 82 (2004) 430–436. https://doi.org/10.1016/j.fertnstert.2004.03.018.
[66] S.A. Dean, J. Tan, E.R. O'Brien, F.H.H. Leenen, 17β-Estradiol downregulates tissue angiotensin-converting enzyme and ANG II type 1 receptor in female rats, American Journal of Physiology-Regulatory, Integrative and Comparative Physiology. 288 (2005) R759–R766. https://doi.org/10.1152/ajpregu.00595.2004.
[67] A.A. Shaikh, Estrone and Estradiol Levels in the Ovarian Venous Blood from Rats During the Estrous Cycle and Pregnancy, Biology of Reproduction. 5 (1971) 297–307. https://doi.org/10.1093/biolreprod/5.3.297.
[68] W.K. Morishige, G.J. Pepe, I. Rothchild, Serum Luteinizing Hormone, Prolactin and Progesterone Levels During Pregnancy in the Rat, Endocrinology. 92 (1973) 1527–1530. https://doi.org/10.1210/endo-92-5-1527.
[69] G.J. Gilson, M.D. Mosher, K.P. Conrad, Systemic hemodynamics and oxygen transport during pregnancy in chronically instrumented, conscious rats., The American Journal of Physiology. 263 (1992) H1911–8. https://doi.org/10.1152/ajpheart.1992.263.6.H1911 [doi].
[70] B.F. Slangen, I.C. Out, C.M. Verkeste, L.L. Peeters, Hemodynamic changes in early pregnancy in chronically instrumented, conscious rats, American Journal of Physiology-Heart and Circulatory Physiology. 270 (1996) H1779–H1784. https://doi.org/10.1152/ajpheart.1996.270.5.H1779.
[71] W.M. Barron, B.A. Stamoutsos, M.D. Lindheimer, Role of volume in the regulation of vasopressin secretion during pregnancy in the rat., J. Clin. Invest. 73 (1984) 923–932. https://doi.org/10.1172/JCI111316.

[72] J.M. Bradley, J.B. Nguyen, A.C. Fournett, J.D. Gardner, Cigarette Smoke Exacerbates Ventricular Remodeling and Dysfunction in the Volume Overloaded Heart, Microsc Microanal. 18 (2012) 91–98. https://doi.org/10.1017/S1431927611012207.
[73] M. Huang, R.L. Hester, A.C. Guyton, Hemodynamic changes in rats after opening an arteriovenous fistula, American Journal of Physiology-Heart and Circulatory Physiology. 262 (1992) H846–H851. https://doi.org/10.1152/ajpheart.1992.262.3.H846.
[74] X. Xu, J.-C. Xiao, L.-F. Luo, S. Wang, J.-P. Zhang, J.-J. Huang, M.-L. Liu, C.-G. Liu, K.-Q. Xu, Y.-J. Li, H.-P. Song, Effects of ovariectomy and 17β-estradiol treatment on the renin–angiotensin system, blood pressure, and endothelial ultrastructure, International Journal of Cardiology. 130 (2008) 196–204. https://doi.org/10.1016/j.ijcard.2007.08.041.
[75] H. Fraser, S.T. Davidge, A.S. Clanachan, Activation of Ca21-independent nitric oxide synthase by 17β-estradiol in post-ischemic rat heart, Cardiovascular Research. (2000) 8.
[76] J.-W. Liu, D.D. Dawson, C.E. Peters, M.A. Baker, A.M. Walker, Estrogen replacement in ovariectomized rats results in physiologically significant levels of circulating progesterone, and co-administration of progesterone markedly reduces the circulating estrogen, Endocr. 6 (1997) 125–131. https://doi.org/10.1007/BF02738955.
[77] B. Xue, J. Pamidimukkala, D.B. Lubahn, M. Hay, Estrogen receptor-α mediates estrogen protection from angiotensin II-induced hypertension in conscious female mice, American Journal of Physiology-Heart and Circulatory Physiology. 292 (2007) H1770–H1776. https://doi.org/10.1152/ajpheart.01011.2005.
[78] A.M.D. Gonzalez, J.C. Osorio, C. Manlhiot, D. Gruber, S. Homma, S. Mital, Hypertrophy signaling during peripartum cardiac remodeling, American Journal of Physiology-Heart and Circulatory Physiology. 293 (2007) H3008–H3013. https://doi.org/10.1152/ajpheart.00401.2007.
[79] K. Lemmens, K. Doggen, G.W. De Keulenaer, Activation of the neuregulin/ErbB system during physiological ventricular remodeling in pregnancy., American Journal of Physiology. Heart and Circulatory Physiology. 300 (2011) H931–42. https://doi.org/10.1152/ajpheart.00385.2010.
[80] Y. Lundgren, K. Karlsson, U. Ljungblad, Changes in central hemodynamics during pregnancy in renal hypertensive rats, Clin Exp Hypertens B. 1 (1982) 441–453. https://doi.org/10.3109/10641958209009618.
[81] M. Jankowski, D. Wang, S. Mukaddam-Daher, J. Gutkowska, Pregnancy alters nitric oxide synthase and natriuretic peptide systems in the rat left ventricle, Journal of Endocrinology. 184 (2005) 209–217. https://doi.org/10.1677/joe.1.05702.
[82] S. Rimbaud, H. Sanchez, A. Garnier, D. Fortin, X. Bigard, V. Veksler, R. Ventura-Clapier, Stimulus specific changes of energy metabolism in hypertrophied heart, Journal of Molecular and Cellular Cardiology. 46 (2009) 952–959. https://doi.org/10.1016/j.yjmcc.2009.01.013.
[83] F.A. Babiker, D. Lips, R. Meyer, E. Delvaux, P. Zandberg, B. Janssen, G. Van Eys, C. Grohé, P.A. Doevendans, Estrogen receptor β protects the murine heart against left ventricular hypertrophy, Arteriosclerosis, Thrombosis, and Vascular Biology. 26 (2006) 1524–1530. https://doi.org/10.1161/01.ATV.0000223344.11128.23.
[84] A. Linke, W. Li, H. Huang, Z. Wang, T.H. Hintze, Role of cardiac eNOS expression during pregnancy in the coupling of myocardial oxygen consumption to cardiac work, American Journal of Physiology-Heart and Circulatory Physiology. 283 (2002) H1208–H1214. https://doi.org/10.1152/ajpheart.00108.2002.

[85] H. Xu, E.D. van Deel, M.R. Johnson, P. Opić, B.R. Herbert, E. Moltzer, S.R. Sooranna, H. van Beusekom, W.-F. Zang, D.J. Duncker, J.W. Roos-Hesselink, Pregnancy mitigates cardiac pathology in a mouse model of left ventricular pressure overload, American Journal of Physiology - Heart and Circulatory Physiology. 311 (2016) H807–H814. https://doi.org/10.1152/ajpheart.00056.2016.
[86] D. Hilfiker-Kleiner, K. Kaminski, E. Podewski, T. Bonda, A. Schaefer, K. Sliwa, O. Forster, A. Quint, U. Landmesser, C. Doerries, M. Luchtefeld, V. Poli, M.D. Schneider, J.-L. Balligand, F. Desjardins, A. Ansari, I. Struman, N.Q.N. Nguyen, N.H. Zschemisch, G. Klein, G. Heusch, R. Schulz, A. Hilfiker, H. Drexler, A Cathepsin D-Cleaved 16 kDa Form of Prolactin Mediates Postpartum Cardiomyopathy, Cell. 128 (2007) 589–600. https://doi.org/10.1016/j.cell.2006.12.036.
[87] M. Maillet, J.H. van Berlo, J.D. Molkentin, Molecular basis of physiological heart growth: fundamental concepts and new players, Nat Rev Mol Cell Biol. 14 (2013) 38–48. https://doi.org/10.1038/nrm3495.

Supplemental Figure 1

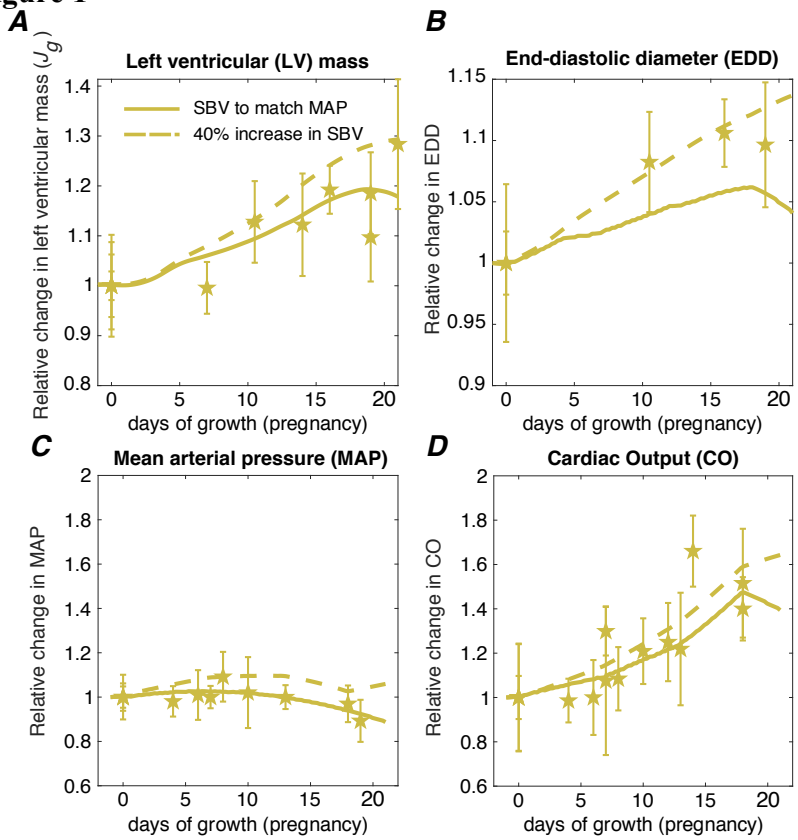

Supplemental Figure 1: When stressed blood volume (*SBV*) is increased 40% linearly over 21 days of growth (dashed lines), the model slightly over predicts growth and mean arterial pressure (MAP), compared to the original simulation where *SBV* was adjusted to match MAP (solid lines). Symbols represent experimental data (See Fig. 8 for references) A.) Relative LV mass increase, B.) Relative change in end-diastolic diameter (EDD), C.) Relative change in mean arterial pressure (MAP), D.) Relative change in cardiac output (CO).